HHS Public Access

Author manuscript

Cell Rep. Author manuscript; available in PMC 2022 December 07.

Published in final edited form as:

Cell Rep. 2022 November 22; 41(8): 111701. doi:10.1016/j.celrep.2022.111701.

En1 and Lmx1b do not recapitulate embryonic dorsal-ventral limb patterning functions during mouse digit tip regeneration

Gemma L. Johnson[1,2], **Morgan B. Glasser**[1], **Julia F. Charles**[1,3], **Jeffrey Duryea**[4], **Jessica A. Lehoczky**[1,5,*]

[1]Department of Orthopedic Surgery, Brigham and Women's Hospital, Boston, MA 02115, USA

[2]Department of Systems Biology, Harvard Medical School, Boston, MA 02115, USA

[3]Department of Medicine, Brigham and Women's Hospital, Boston, MA 02115, USA

[4]Department of Radiology, Brigham and Women's Hospital, Boston, MA 02115, USA

[5]Lead contact

SUMMARY

The mouse digit tip regenerates following amputation. How the regenerate is patterned is unknown, but a long-standing hypothesis proposes developmental patterning mechanisms are re-used during regeneration. The digit tip bone exhibits dorsal-ventral (DV) polarity, so we focus on En1 and Lmx1b, two factors necessary for DV patterning during limb development. We investigate whether they are re-expressed during regeneration in a developmental-like pattern and whether they direct DV morphology of the regenerate. We find that both En1 and Lmx1b are expressed in the regenerating digit tip epithelium and mesenchyme, respectively, but without DV polarity. Conditional genetics and quantitative analysis of digit tip bone morphology determine that genetic deletion of En1 or Lmx1b in adult digit tip regeneration modestly reduces bone regeneration but does not affect DV patterning. Collectively, our data suggest that, while En1 and Lmx1b are re-expressed during mouse digit tip regeneration, they do not define the DV axis during regeneration.

Graphical Abstract

*Correspondence: jlehoczky@bwh.harvard.edu.

AUTHOR CONTRIBUTIONS

G.L.J., J.F.C., J.D., and J.A.L. conceptualized and designed the experiments. G.L.J., M.B.G., and J.A.L. performed the experiments and acquired the data. G.L.J., M.B.G., J.D., and J.A.L. analyzed the data. G.L.J. and J.A.L. wrote the manuscript. All authors edited the manuscript.

SUPPLEMENTAL INFORMATION

Supplemental information can be found online at https://doi.org/10.1016/j.celrep.2022.111701.

DECLARATION OF INTERESTS

The authors declare no competing interests.

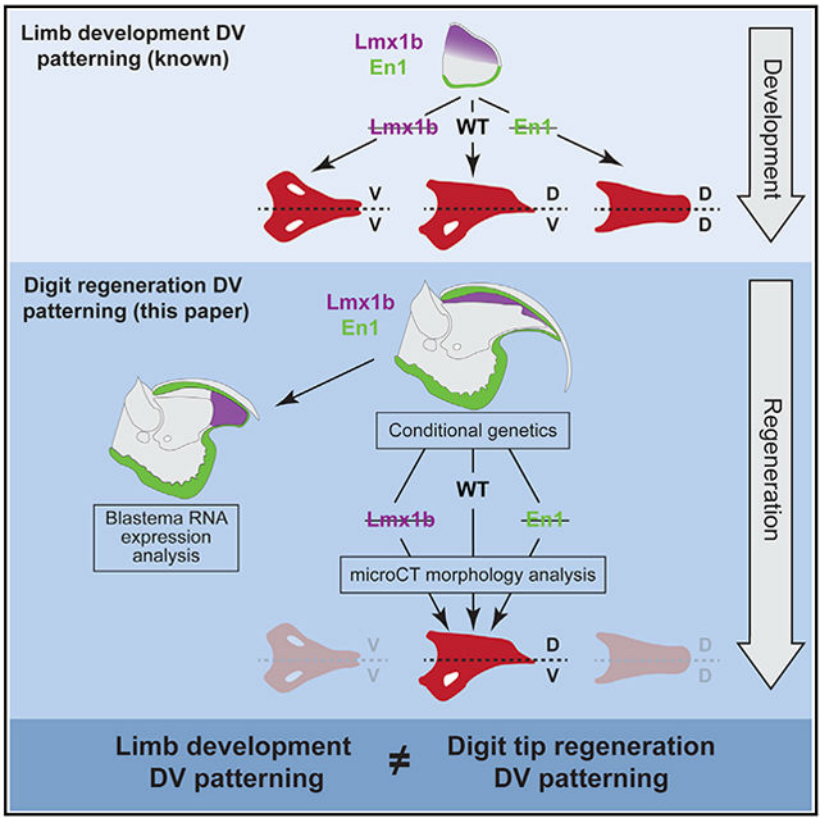

In brief

Johnson et al. find dorsal-ventral (DV) genes En1 and Lmx1b are expressed in regenerating mouse digit tips, but without DV polarity. Conditional genetics and bone morphology analyses indicate En1 or Lmx1b do not alter regenerated digit DV patterning, refuting the hypothesis that embryonic limb patterning pathways are re-used during regeneration.

INTRODUCTION

Some tetrapods, including salamanders, newts, and juvenile xenopus, are able to regenerate entire limbs after amputation, and several species of fish, exemplified by zebrafish, are capable of fin regeneration.[1,2] Humans and mice do not regenerate limbs but do innately regenerate amputated digit tips, the most distal structures of the limb.[3-5] Limb and appendage regeneration in all of these models requires the blastema, a collection of proliferating progenitor cells that forms underneath the wound epithelium covering the amputation site.[6-8] This blastema grows and differentiates into a new limb or appendage which re-establishes the correct three-dimensional pattern and tissue organization of the original structure in the proximal-distal (PD), anterior-posterior (AP), and dorsal-ventral (DV) axes. However, despite extensive study in salamanders, it remains unclear how the correct patterning is restored in the regenerating limb (reviewed in Vieira and McCusker[9] and Flowers and Crews[10]).

Embryonic limb development is a well-studied model of how multipotent mesenchyme differentiates into the tissues of the mature limb in a stereotyped three-dimensional pattern. Because there are strong similarities in terms of tissue types and their interactions, the process of limb regeneration is often compared with embryonic limb development, which provides a useful lens for studying morphogenesis during regeneration.[11] The developing limb bud is comprised of undifferentiated mesenchymal cells surrounded by the apical ectodermal ridge (AER), a specialized distal epithelium that is integral for the proliferation and differentiation of the underlying mesenchyme.[12,13] As with the developing limb bud, the regenerative blastema in salamander, frog, and mouse is largely made up of mesenchymal cells that are surrounded by a specialized distal epithelium, the wound epithelium, that signals to the underlying mesenchyme.[14-21] Furthermore, in both limb development and regeneration, progenitor cells proliferate and re-pattern to form a structure that is the correct size and shape in comparison with the rest of the organism. Beyond tissue types and morphology, there is also evidence for shared gene expression patterns between limb regeneration and development. In the axolotl, posterior HoxA genes are re-expressed during limb regeneration in the same spatial and temporal pattern as during limb development.[22,23] In mice, Fgf2 is expressed in the AER as well as in the wound epithelium of regenerating digit tips.[24] In addition, the cell types involved in limb development and regeneration have been compared by single-cell RNA sequencing (scRNA-seq) analyses in several model systems.[15,16,25] In mice, for example, a subset of mesenchymal digit tip blastema cells do express embryonic limb development-related genes, such as Hoxa13 and Hoxd13, as well as many genes related to ossification,[15,26] but their overall transcriptional profiles are not equivalent to those of embryonic limb bud cells.[15] The mouse wound epithelium has not been directly compared with the AER. However, the specialized wound epithelium during frog regeneration is transcriptionally similar to the AER.[16] While these studies show developmental limb patterning genes are re-expressed during regeneration, it remains unknown whether they have the same functional role in regeneration as they do in development.

Mouse digit tip regeneration is a human-relevant model to dissect the role of limb development genes during regeneration at a genetic and functional level. The digit tip is a distal limb structure comprised of different tissue types, including bone, connective tissue, blood vessels, nerves, epithelium, and the nail. Amputating the distal mouse digit tip results in a stereotyped regenerative process, which includes formation of a blastema made up of different cell types, including a heterogeneous population of fibroblasts, pre-osteoblasts, Schwann cells, immune cells, and vascular smooth muscle and endothelial cells.[15,27-30] While the digit tip blastema is not identical in cell type to mouse embryonic limb bud cells,[15] it remains to be determined if blastema cells are under the influence of limb development molecular pathways in the patterning of the regenerating digit tip. For example, genes necessary for embryonic limb patterning may be re-deployed in morphogenesis of the regenerating mouse digit tip.

In this paper, we expand the comparison of mouse digit tip regeneration to limb development through the lens of patterning. Of the PD, AP, and DV axes, the digit tip bone has the most phenotypic variation in the DV axis. We exploit the DV bone morphology to investigate the role of Engrailed 1 (En1) and Lim homeobox transcription factor 1 beta (Lmx1b), two

transcription factors necessary for DV patterning in the developing limb bud, during digit tip regeneration. Using RNA *in situ* hybridization, we define the expression domains of En1 and Lmx1b during digit development and regeneration, showing that En1 and Lmx1b are expressed during mouse digit tip regeneration but with no DV restriction. Conditional genetics and computational analysis of microCT scans of 515 digit tip bones enable us to determine that loss of En1 or Lmx1b modestly impairs bone regeneration but does not alter the DV morphology of regenerated digit tip bones. Taken together, our data show that En1 and Lmx1b do not direct DV patterning during digit tip regeneration, challenging a long-standing hypothesis that regeneration re-deploys developmental patterning genes.[11]

RESULTS

Dorsally restricted Lmx1b expression persists throughout digit development while En1 expression is dynamic

The expression domains of En1 and Lmx1b in early mouse limb development are well described. Lmx1b expression is restricted to the dorsal limb bud mesenchyme by embryonic day 10.5 (E10.5)[31,32] (Figures S1A, S1B, and S1B''). This expression persists in the dorsal mesenchyme of the distal autopod, including the digit, until at least E16.5.[33] Whether Lmx1b expression in the digit persists after E16.5, and in which tissues, is not reported. Separately, it has been established that En1 is expressed in the ventral limb bud epithelium by E9.5, as soon as the limb bud is formed[34] (Figures S1A, S1B, and S1B''). En1 continues to be expressed in the digit epithelium until at least E13.5,[32] but the expression pattern of En1 in the digit after this stage is not reported. However, defining dorsal features of the ectoderm, such as the nail fold and matrix, do not begin to develop until E16.5, and the nail plate itself is not present until E18.5.[35] Similarly, the ventral toe pad and the distal phalanx do not begin forming until E14.5.[36,37] To determine if expression of En1 and Lmx1b persists in the developing digit tip and if they maintain embryonic limb bud DV restriction, we used hybridization chain reaction RNA fluorescent *in situ* hybridization (HCR RNA-FISH)[38] with probes to Lmx1b and En1 in E16.5 (embryonic), postnatal day 4/5 (PN4/5; neonatal), and 6-week-old (adult) digits (Figure 1A). HCR RNA-FISH in the E16.5 digit shows that En1 is expressed in the ventral epithelium (Figures 1D and 1D') with some expression dorsal to the DV boundary at the distal tip of the digit (Figures 1C and 1C'), but not in the rest of the dorsal epithelium (Figures 1B and 1B'). By PN4/5, epithelial En1 expression is maintained ventrally (Figures 1G and 1G') and at the distal tip (Figures 1F and 1F') and has expanded further dorsally (Figures 1E and 1E') but does not yet reach the nail matrix, a more proximal region of the dorsal epithelium (not shown). In the adult digit, no DV En1 restriction is found, and expression is detected throughout the entirety of the digit tip epithelium (Figures 1H'-1J'). Thus, En1 is expressed exclusively in the epithelium, and the original ventral expression domain expands dorsally as the digit matures.

Conversely, we find that Lmx1b is expressed in the dorsal (Figures 1B and 1B'') but not distal (Figures 1C and 1C'') or ventral (Figures 1D and 1D'') mesenchyme in the E16.5 digit. In the neonatal digit, Lmx1b continues to be expressed in dorsal mesenchyme (Figures 1E and 1E'') but not at the distal tip of the digit (Figures 1F and 1F'') or ventrally (Figures 1G and 1G''). Similarly, in the adult digit tip, Lmx1b is expressed in the dorsal mesenchyme

(Figures 1H and 1H’’) and has extended more distally to the tip (Figures 1I and 1I’’) but is not expressed in the ventral mesenchyme (Figures 1J and 1J’’). At all these developmental stages, Lmx1b is expressed only in mesenchymal cells and not in the epithelium (Figures 1A and 1B’’-1J’’).

During mouse limb development, En1 and Lmx1b are part of a network of gene expression that includes Wnt7a.[39-42] En1 is expressed in the ventral epithelium and downregulates Wnt7a, leading to Wnt7a expression only in the dorsal epithelium. Wnt7a then induces Lmx1b expression in the adjacent dorsal mesenchyme (Figure S1A). Wnt7a was detected in the epithelium of control E12.5 forebrain sections by HCR RNA-FISH (Figures S3A and S3A’) in contrast to the no probe control section (Figure S3B). HCR RNA-FISH of adult digits for Wnt7a shows no expression in the epithelium or otherwise in the adult digit (Figures S3D-S3G). Taken together, our data show that expression of both En1 and Lmx1b persists throughout digit development and into adult digit homeostasis, whereas Wnt7a expression is undetectable in the adult. Despite the change in the En1 expression domain throughout development of the digit tip, En1 remains restricted to the epithelium, as in early limb bud development, and Lmx1b remains restricted to the mesenchyme.

En1 and Lmx1b are expressed in the regenerating digit tip without DV polarity

En1 and Lmx1b expression persists into adulthood in the digit tip in the same tissue compartments as during limb development (Figure 1), suggesting that they could function in DV patterning during digit tip regeneration. To address this, we first turned to our scRNA-seq data from adult mouse regenerating digit tips (accession number GSE143888[27]) to determine if En1 and Lmx1b are expressed during digit tip regeneration. Combining scRNA-seq data from 11, 12, 14, and 17 days postamputation (dpa) and unamputated (UA) controls, 95.4% of cells expressing En1 are epithelial and 95.1% of cells expressing Lmx1b are fibroblasts (98.7% are of general mesenchymal origin) (Figures 2A and 2B), consistent with their tissue specificity during limb development. To assess any spatial restriction of En1 and Lmx1b expression during regeneration and whether it recapitulates that of early limb development, we utilized HCR RNA-FISH for Lmx1b and En1 in the regenerating digit tip at 11 dpa (Figures 2D-2I). 11 dpa represents an early stage of regeneration when the blastema has formed but there is no widespread differentiation (Figure 2C, middle).[28] Consistent with the scRNA-seq data, HCR RNA-FISH shows that En1 is expressed contiguously throughout the dorsal and ventral epithelium of the regenerating digit tip (Figures 2D, 2D’, 2F, and 2F’). En1 expression is also present in the epithelium at the distal tip surrounding the blastema (Figures 2E and 2E’), and thus deviates from the DV spatial restriction found in the embryonic limb bud. This suggests that the function of En1 in regeneration could be discrete from that of limb development.

By HCR RNA-FISH, Lmx1b is heterogeneously expressed at a low level in cells throughout the blastema at 11 dpa and not found in the epithelium (Figures 2G-2I). Lmx1b is expressed by cells in the dorsal blastema (Figures 2G and 2G’) as well as the central (Figures 2H and 2H’) and ventral (Figures 2I and 2I’) regions of the blastema. This pattern holds through later stages of digit tip regeneration: Lmx1b continues to be expressed dorsally (Figures S2A, S2A’, S2D, and S2D’), centrally (Figures S2B, S2B’, S2E, and S2E’), and

ventrally (Figures S2C, S2C', S2F, and S2F') throughout the mesenchyme of the blastema at both 14 dpa (Figures S2A-S2C) and 17 dpa (Figures S2D-S2F). This is in contrast to embryonic limb bud and adult homeostatic digit Lmx1b expression, which is restricted to the dorsal mesenchyme, suggesting a regeneration-specific role for Lmx1b. However, Lmx1b is expressed in the mesenchyme, a tissue type consistent with limb bud development and our digit tip scRNA-seq data. In contrast to early limb development (Figure S1A), Wnt7a expression was not detected in the epithelium of either UA or 11 dpa regenerating digit tips (Figures S3H-S3K), confirming the lack of Wnt7a expression found in the scRNA-seq data from combined epithelium of UA and regenerating digit tips[27] (Figure S3C). These expression studies suggest that the embryonic limb DV patterning network is not re-deployed during digit tip regeneration to direct DV morphogenesis.

Embryonic loss of En1 and Lmx1b results in dysmorphic digits and affects digit tip regeneration

To functionally test if En1 or Lmx1b are necessary for DV patterning during digit xtip regeneration, we utilized tissue-specific conditional genetics. We first bred En1-flox;K14-cre mice, which have genetic deletion of En1 in the epithelium.[43,44] As reported previously, embryonic loss of En1 in the epithelium results in limbs absent of ventral structures and with duplicated dorsal structures, such as hair follicles on the palm and nails extending to the ventral digit[41] (Figures 3A and 3D). Consistent with this phenotype, En1-fl/fl;K14-cre digit tip bones are cylindrical, exhibiting "double dorsal" morphology and a loss of ventral structures, such as the sesamoid bone and ventral hole (Figure 3E) compared with En1-wt/wt;K14-cre digits (Figure 3B). To determine the effect of developmental loss of En1 on digit tip regeneration, we amputated these digits at PN3 and evaluated regenerated digit tip bones at 3 weeks post amputation (wpa). We calculated the percent regeneration by dividing regenerated digit length by the same animal's contralateral UA digit length. Both En1-fl/fl;K14-cre and En1-wt/wt;K14-cre digit tip bones regenerated following amputation (Figures 3C and 3F). The En1-fl/fl;K14-cre regenerated digits had a higher percent regeneration in length than the wild-type controls (Figure 3M) and appear to regenerate with double dorsal morphology (Figure 3F). However, because the digit tip bone was dysmorphic in the DV axis before amputation, it is unclear whether the aberrant regenerated bone morphology is due to loss of En1 or due to the pre-existing morphology of the bone and surrounding tissues.

We next bred Lmx1b-flox;Prx1-cre mice, which have genetic deletion of Lmx1b in the developing limb.[45,46] Consistent with previous reports, genetic deletion of Lmx1b in the limb results in aberrant DV limb morphology.[47] Compared with control Lmx1b-fl/wt;Prx1-cre digits (Figures 3G and 3H), Lmx1b knockout (KO) mice exhibit loss of dorsal structures, such as the nail, and gain of ectopic ventral structures, such as the toe pad on the dorsal side of the digit (Figure 3J). Similarly, the digit tip bones show a "double ventral" phenotype exemplified by an ectopic sesamoid bone and bone hole on the dorsal side (Figure 3K). To test the necessity of Lmx1b for DV morphology in digit tip regeneration we amputated the digit tips of Lmx1b-fl/fl;Prx1-cre PN3 mice and Lmx1b-fl/wt;Prx1-cre controls. At 3 wpa, Lmx1b-fl/wt;Prx1-cre control digit bones regenerate normally (Figure 3I), whereas Lmx1b-fl/fl;Prx1-cre digit tip bones do not regenerate (Figures 3L and 3N). This suggests

that Lmx1b is necessary in the mesenchyme for digit tip regeneration. However, Lmx1b-fl/fl;Prx1-cre mice have reduced or absent nails (Figure 3J), a dorsal structure that is necessary for regeneration,[4,48] so the genetic necessity of Lmx1b for regeneration in this experiment is confounded.

Conditional deletion of En1 and Lmx1b during regeneration causes modest bone loss

To disentangle the developmental digit tip bone morphologies from any regenerative phenotype, we conditionally deleted En1 and Lmx1b in adult mice with normally developed limbs. We first bred En1 epithelial-specific conditional KO (cKO) mice using an En1-floxed allele[43] and a K14-creERT2 tamoxifen-inducible cre allele[49] (Figure 4A). To test the role of En1 during adult digit tip regeneration, we induced recombination in En1-fl/fl;K14-creERT2 mice with tamoxifen and compared them with untreated En1-fl/fl and En1-fl/fl;K14-creERT2 control cohorts. Tamoxifen dosing was sufficient for recombination of the En1 locus as determined by qPCR of genomic DNA and HCR RNA-FISH utilizing a probe specific to the recombined portion of the En1 transcript (Figures S4E-S4G). In addition to the expected recombination in En1-fl/fl;K14-creERT2 + tamoxifen animals, we also detected ectopic genomic recombination in uninduced En1-fl/fl;K14-creERT2 mice (Figure S4E). This genotypic finding is consistent with the uninduced En1-fl/fl;K14-creERT2 phenotype, whereby around 5 weeks of age En1-fl/fl;K14-creERT2 mice, regardless of tamoxifen induction, develop ectopic ventral nail-like structures from their toe pads (Figures S4A and S4B). Despite the leaky cre affecting ectodermal structures in the digit tip, the bone morphology remains comparable with En1-fl/fl mice, with no evidence of aberrant DV patterning (Figures 4B, 4D, S4C, and S4D). To keep the amputation plane consistent, we amputated En1-fl/fl;K14-creERT2 digits when the mice were 4 weeks old, before the leaky cre phenotype appears. Digit tips of 4-week-old mice were amputated 1 day after the last tamoxifen dose and collected at 4 wpa, when adult digit tip bone regeneration is complete, and scanned by micro-computed tomography (uCT) to evaluate bone regeneration (Figure 4A).[28,50]

By 4 wpa, both En1-fl/fl;K14-creERT2 induced and En1-fl/fl control digit tip bones successfully regenerated, as grossly assessed from uCT renderings (Figures 4C and 4E). Quantification of length and volume provided more detailed metrics of the regenerated bones. In agreement with previous analyses of wild-type digit tip bone length and volume after regeneration by uCT,[28,50] the regenerated En1-fl/fl control digits have an over-regeneration of bone length ($p = 1.5 \times 10^{-4}$) and volume ($p < 1 \times 10^{-7}$) compared with the UA contralateral controls (Figures 4J and 4K). En1-fl/fl;K14-creERT2 + tamoxifen 4 wpa digits have a reduction in length ($p < 1 \times 10^{-7}$) and volume ($p < 1 \times 10^{-7}$) compared with regenerated En1-fl/fl control digits (Figures 4J and 4K). Uninduced En1-fl/fl;K14-creERT2 digits also exhibit reduced regenerative length ($p = 0.001$) and volume ($p = 2.5 \times 10^{-6}$) compared with En1-fl/fl control digits, consistent with the ectopic recombination found in these digits (Figures 4J, 4K, S4B, and S4E). To ensure that tamoxifen itself is not causing this bone regeneration phenotype, we administered tamoxifen to a cohort of En1-fl/fl mice. These digits show no significant difference in bone length or volume when compared with control digits at either UA or 4 wpa, and they over regenerate to a longer length ($p = 5.1 \times 10^{-3}$) and volume ($p = 1.4 \times 10^{-6}$) when compared with UA digits in the same condition

(Figures 4J and 4K). The En1-fl/fl + tamoxifen digits also regenerate to a significantly higher length than En1-fl/fl;K14-creERT2 ($p = 4.1 \times 10^{-2}$) and a higher length and volume than En1-fl/fl;K14-creERT2 + tamoxifen (length, $p = 4.1 \times 10^{-5}$; volume, $p = 7.4 \times 10^{-3}$) digits (Figures 4J and 4K), demonstrating that the bone regeneration phenotype is not due to tamoxifen. These data show that loss of En1 in the epithelium during regeneration does not affect UA digit bone length or volume but leads to a modest inhibition of bone regeneration.

We next bred Lmx1b mesenchymal-specific conditional KO mice using an Lmx1b-flox allele and the Msx1-creERT2 tamoxifen-inducible cre allele.[45,51] Previous work has shown Msx1 is expressed in all fibroblasts in the digit tip, so Msx1-creERT2 should recombine any blastema cells expressing Lmx1b.[27] To determine the role of Lmx1b in digit tip regeneration, we induced recombination in Lmx1b-fl/fl;Msx1-creERT2 mice with tamoxifen while leaving Lmx1b-fl/fl and Lmx1b-fl/fl;Msx1-creERT2 control cohorts uninduced. Tamoxifen dosing was sufficient to induce recombination of the Lmx1b locus, demonstrated by qPCR of genomic DNA and qRT-PCR of 12 dpa blastema RNA using probes for a deleted portion of the Lmx1b RNA (Figures S4H and S4I). No ectopic recombination was detected in the control cohorts using these methods (Figures S4H and S4I). We collected regenerated digit tips at 4 or 6 wpa and performed uCT analyses to determine bone length and volume.

Gross qualitative assessment of the uCT scans showed that both Lmx1b-fl/fl;Msx1-creERT2 + tamoxifen and Lmx1b-fl/fl control digit tip bones regenerated (Figures 4F-4I). Quantitative analysis found that Lmx1b-fl/fl control regenerated digit tips are longer at 4 wpa ($p = 0.024$) than contralateral UA controls, which is consistent with over-regeneration of the En1 control digits and previous literature (Figures 4J and 4L).[28,50] Uninduced Lmx1b-fl/fl;Msx1-creERT2 digits regenerate to a length equivalent to Lmx1b-fl/fl control digits, while Lmx1b-fl/fl;Msx1-creERT2 + tamoxifen regenerated digits are shorter at both 4 wpa ($p = 1.0 \times 10^{-7}$) and 6 wpa ($p = 8.6 \times 10^{-4}$) compared with Lmx1b-fl/fl control digits (Figure 4L). Lmx1b-fl/fl;Msx1-creERT2 + tamoxifen UA digits are also shorter than Lmx1b-fl/fl control UA digits ($p = 0.049$), implying that loss of Lmx1b may disrupt bone homeostasis. In terms of volume, Lmx1b-fl/fl control digits have a larger volume at 4 wpa ($p < 1 \times 10^{-7}$) and 6 wpa ($p < 1 \times 10^{-7}$) than UA, as expected and consistent with over-regeneration (Figure 4M). Uninduced Lmx1b-fl/fl;Msx1-creERT2 digits at 4 wpa have not regenerated to the Lmx1b-fl/fl control volume ($p = 0.010$), but catch up by 6 wpa, while Lmx1b-fl/fl;Msx1-creERT2 + tamoxifen digits have less volume at both 4 wpa ($p = 3.7 \times 10^{-5}$) and 6 wpa ($p = 6.1 \times 10^{-5}$) compared with Lmx1b-fl/fl controls (Figure 4M). These data indicate that mesenchymal Lmx1b is not required for digit tip bone regeneration, but loss of Lmx1b during regeneration does modestly impair bone regeneration. Therefore, the loss of regenerative ability in the Lmx1b developmental knockout (Lmx1b-fl/fl;Prx1-cre, Figure 3) can be attributed to the pre-existing digit dysmorphology, not the necessity of Lmx1b for regeneration.

En1 and Lmx1b do not regulate DV bone patterning during digit tip regeneration

While our data find that Lmx1b and En1 are not genetically necessary for successful digit tip regeneration, we sought to determine if they are necessary for patterning the DV axis of the

regenerating digit tip. The loss of En1 during limb development results in a double dorsal digit tip bone with a conical morphology (Figures 3E and 5B). To quantify the circularity of this morphology, we calculated the aspect ratio of uCT sections transecting the DV axis. The ratio of bone width and height were measured in the uCT sections, where an aspect ratio of 1 reflects a more circular shape (Figure 5A). It follows that uCT sections through the length of an En1-fl/fl;K14-cre neonatal digit tip bone have aspect ratios closer to 1 (Figures 5B and 5C) than comparable sections through an En1-fl/fl control digit tip bone (Figures 5D and 5E). The average aspect ratio of En1-fl/fl;K14-cre developmental knockout UA (0.86 ± 0.10) and regenerated (0.86 ± 0.10) digit tip bones are near 1 throughout the length of the digit tip, with no significant difference in ratio among the slices (Figure 5C). No significant difference in the aspect ratio was found between the En1-fl/fl;K14-cre UA and regenerated digit uCT slices, supporting our 2D qualitative assessment (Figure 3F) that the regenerated digit maintains the double dorsal cylindrical morphology of the UA digit (Figure 5C).

In the adult En1 cKO model, UA En1-fl/fl control (0.68 ± 0.11), uninduced En1-fl/fl;K14-creERT2 (0.61 ± 0.09), and En1-fl/fl;K14-creERT2 + tamoxifen (0.61 ± 0.13) digits have smaller aspect ratios than the En1-fl/fl;K14-cre developmental knockout (Figure 5E), consistent with non-circular morphology. Despite variability in the aspect ratio measurement at the tip of the UA digit, En1-fl/fl digits have larger aspect ratios than En1-fl/fl;K14-creERT2 digits at 45% ($p = 0.006$), 55% ($p = 0.042$), 65% ($p = 0.002$), and 75% ($p = 8.1 \times 10^{-6}$) of the digit tip length, and En1-fl/fl;K14-creERT2 + tamoxifen digits at 65% ($p = 0.002$) and 75%($p<1 \times 10^{-7}$) of digit length (Figure 5E top). This likely reflects stochasticity in the shape of the digit bone near the tip. If En1 regulates DV patterning during regeneration, we would expect the regenerated bone in En1-fl/fl;K14-creERT2 + tamoxifen digits to have a circular, double dorsal, morphology. However, the average aspect ratios for En1-fl/fl control (0.56 ± 0.15), uninduced En1-fl/fl;K14-creERT2 (0.53 ± 0.10), and En1-fl/fl;K14-cre-ERT2 + tamoxifen (0.60 ± 0.16) regenerated digits are similar, with no significant differences in aspect ratio at any slice (Figure 5E, bottom). Overall, this analysis shows that deletion of En1 during regeneration does not lead to a circular, double dorsal bone morphology, and thus En1 does not specify ventral fate during digit tip regeneration.

More generally, loss of En1 and Lmx1b during limb development result in near perfect DV symmetry throughout the digit tip bone (Figures 3E and 3K). If En1 or Lmx1b are involved in DV patterning of the regenerating digit tip, then loss of either during regeneration should increase DV symmetry in the regenerated digit bone. To measure DV symmetry, we placed landmarks at the most dorsal and most ventral points on a fixed slice on each uCT scan (Figure 6A, red cubes) and used this index slice to bisect the digit into dorsal and ventral compartments (Figure 6A). We measured the dorsal and ventral areas progressively from the index slice to the distal tip, computed the ventral to dorsal area ratio as a measure of symmetry (Figure 6A), and plotted the ratio for each slice as a function of normalized position along the digit tip bone (Figures S5A and S5B). The resulting curve shows a stereotyped shape where segment 1 (s1, Figure 6A) corresponds to the morphology of the proximal digit, the change point corresponds to where the ventral volume of the digit stops decreasing (which is also where the amputation plane is located) (cp, Figure 6A), and the second segment corresponds to the morphology of the regenerated part of the digit when

amputated (s2, Figure 6A). To determine if these parameters significantly change after regeneration in the En1 or Lmx1b cKO models, we used the mcp R package[52] to fit a segmented linear regression model for each digit. The resulting model estimates parameters that describe the slope of s1, the change point position, and the slope of s2.

After fitting a segmented line to each individual digit, we compared the biologically meaningful parameters between groups to determine if the DV morphology of the bone is changed. We find that En1-fl/fl;K14-creERT2 + tamoxifen digit tips are not significantly different than En1-fl/fl control UA digits in either the change point position or the slope of segment 2 (MANOVA, $p = 0.48$) (Figures 6B and 6C), illustrating that loss of En1 in the epithelium does not change the morphology of the digit tip bone during homeostasis. Furthermore, the change points and segment 2 slopes of 4 wpa regenerated En1-fl/fl;K14-creERT2 + tamoxifen digits are not significantly different from En1-fl/fl control 4 wpa digits; the same is true for uninduced, but leaky, En1-fl/fl;K14-creERT2 digits at both UA and 4 wpa time points (MANOVA, $p = 0.48$) (Figures 6B and 6C). This suggests that loss of En1 in the epithelium during regeneration does not change the morphology or DV symmetry of the regenerated digit tip, further underscoring that En1 does not participate in DV patterning during digit tip regeneration.

We performed the same DV symmetry analysis for Lmx1b cKO mutants and controls. No significant difference was found in change point position or segment 2 slope between Lmx1b-fl/fl control and Lmx1b-fl/fl;Msx1-creERT2 uninduced UA digits (cp, $p = 0.21$; s2 slope ANOVA, $p = 0.59$). The same was true when comparing Lmx1b-fl/fl control and Lmx1b-fl/fl;Msx1-creERT2 + tamoxifen (cp, $p = 1$; s2 slope ANOVA, $p = 0.59$) UA digits, which indicates that loss of Lmx1b does not change homeostatic digit morphology (Figures 6D and 6E). Similarly, at 4 wpa, Lmx1b-fl/fl;Msx1-creERT2 uninduced and + tamoxifen digits have no difference in either change point ($p = 0.97$ and $p = 0.99$, respectively) or segment 2 slope (ANOVA, $p = 0.59$) compared with Lmx1b-fl/fl 4 wpa controls (Figures 6D and 6E). By 6 wpa, Lmx1b-fl/fl;Msx1-creERT2 uninduced and + tamoxifen digits also do not have significantly different change point ($p = 0.61$ and $p = 0.99$, respectively) or segment 2 slope (ANOVA, $p = 0.59$) compared with Lmx1b-fl/fl controls (Figures 6D and 6E), indicating that loss of Lmx1b does not change DV morphology in the UA or regenerated digit tip. Interestingly, the segment 1 slope, which corresponds to morphology of the proximal digit tip, is significantly increased at 4 wpa ($p < 1 \times 10^{-7}$) and 6 wpa ($p = 0.007$) compared with UA for both Lmx1b-fl/fl;Msx1-creERT2 + tamoxifen digits ($p < 1 \times 10^{-7}$ and $p = 1.2 \times 10^{-4}$, respectively) as well as Lmx1b-fl/fl control digits ($p < 1 \times 10^{-7}$ and $p = 0.007$, respectively) (Figure S5C). This suggests that both the control and cKO regenerated digits have more ventral bone proximal to the amputation plane in the regenerated digits, but this phenotype is not Lmx1b specific. We hypothesize that the mixed background strains of the Lmx1b-flox and Msx1-creERT2 alleles may promote extended histolysis following amputation, which would cause bone regeneration to also occur more proximally.[53,54] The increase in the measured change points of Lmx1b-fl/fl digits at 4 wpa compared with UA ($p = 0.004$) could be caused by an increase in uncertainty in modeling the change point because the slopes of s1 and s2 are more similar (Figure S5B). Overall, we find that loss of Lmx1b in the mesenchyme during regeneration does not affect the DV symmetry of the digit tip.

DISCUSSION

Recapitulation of developmental gene expression has long been hypothesized to be the mechanism of pattern formation during regeneration.[11] We tested this hypothesis by investigating whether En1 and Lmx1b, two transcription factors necessary for DV patterning during limb development, are also necessary for DV patterning during mouse digit tip regeneration. We show that En1 and Lmx1b are expressed during digit tip regeneration but not with DV polarity. Furthermore, using conditional deletion during regeneration, we show that En1 and Lmx1b are not genetically necessary for DV patterning during mouse digit tip regeneration. This is unexpected given that, in other models of regeneration, particularly zebrafish fin or salamander limb regeneration, developmental patterning genes are expressed in domains similar to development.[22,23,55-58]

If not recapitulating the developmental patterning function, what is the function of En1 or Lmx1b during digit homeostasis and regeneration? Our finding that deletion of En1 in the epithelium during homeostasis results in the ventral toe pad transforming to a dorsal nail-like structure (En1-fl/fl;K14-creERT2; Figure S4B) suggests that En1 continues to play a role in maintaining ventral identity in the epithelium and ectodermal appendages of the adult homeostatic digit. However, since En1 is expressed in both ventral and dorsal epithelium in the adult mouse, which is distinct from limb development, another factor in the epithelium may modulate the maintenance of ventral identity by En1. Beyond DV identity, our data suggest that En1 expression in the epithelium supports bone regeneration because En1-fl/fl;K14-creERT2 regenerated digits had a modest reduction in bone length and volume. This would be an indirect effect because En1 is expressed in the epithelium, although there is evidence that signaling in the nail epithelium can affect bone growth and maintenance as well as regeneration.[24,59]

Digit tip regeneration is closely linked to the nail: amputation proximal to the nail fails to regenerate, and Wnt signaling from the nail bed promotes regeneration.[4,24,48,60] Here, we show that En1-fl/fl;K14-cre regenerated digit tips, with nails encircling the entire digit, regenerate to a greater length than controls (Figure 3M). This is not seen in En1-fl/fl;K14-creERT2 mice, which have a slight reduction of bone length after regeneration (Figure 4J). These seemingly opposite regenerative responses may be attributed to differences in the nail, which is circumferential in En1-fl/fl;K14-cre mice and normal in En1-fl/fl;K14-creERT2 mice. It follows that the nail epithelium may provide a pro-regenerative signal or that the nail plate itself may be integral to patterning the bone during digit tip regeneration by exerting a mechanical force on the tissue.[61,62]

The role of Lmx1b in digit homeostasis and regeneration is less clear. During homeostasis, Lmx1b expression is restricted to the dorsal mesenchyme, which lies beneath the nail epithelium. The nail has been shown to modulate digit tip regeneration partly through Wnt signaling.[24,60] During limb development, Lmx1b is downstream of Wnt7a. While Wnt7a is not expressed in the epithelium of homeostatic or regenerating digit tips (Figure S3), another Wnt ligand expressed in the epithelium may induce Lmx1b expression in the digit tip mesenchyme. The developmental function of Lmx1b suggests that it could function in maintaining the dorsal identity of the nail epithelium during homeostasis, although we do

not find transformation or loss of the nail in our Lmx1b conditional mutants up to 4 weeks after tamoxifen administration.

Furthermore, we find that conditional deletion of Lmx1b results in a modest reduction in bone regeneration. In contrast, Lmx1b has previously been characterized as anti-osteogenic during calvarial development, where Lmx1b is expressed in a population of mesenchymal cells in the suture and loss of Lmx1b results in premature suture closure.[63] Lmx1b is also expressed in the joint mesenchyme surrounding the bone during mouse limb development and zebrafish fin regeneration.[33,64] While our results seem contrary to these findings, it is possible that Lmx1b has a similar anti-osteogenic function in mouse digit tip regeneration. Loss of Lmx1b in blastema cells could cause premature osteogenic differentiation during regeneration, thereby disrupting regeneration and causing loss of regenerated bone length and volume. Alternatively, Lmx1b could have a separate function in the context of adult digit tip homeostasis and regeneration. Loss of Lmx1b also results in shorter digit tip bones independent of regeneration, pointing to a general role in bone homeostasis and maintenance.

By visual inspection, the imperfect regeneration of the digit tip bone could be interpreted as evidence that there is no pre-determined pattern that forms during regeneration. However, our uCT analysis shows that there is a reproducible DV pattern in the regenerated digit tip bone. Our data show that developmental DV patterning genetic networks are not reused during adult digit tip regeneration, which suggests that other factors regulate DV patterning during regeneration. It is difficult to determine candidates for other factors based on limb development alone, because effectors of DV pattern downstream of En1 are largely unknown. ChIP-seq for targets of Lmx1b during limb development has identified many regulatory targets of Lmx1b, but how these genes drive morphological differences is not understood.[65] That said, expression of Lmx1b throughout the blastema could suggest that the blastema is an entirely dorsal structure. However, other experimental evidence does not support this idea. Hyperbaric oxygen treatment causes degradation of the digit tip bone almost entirely after amputation in some cases.[54] If the blastema were entirely dorsal, the regenerated bone would not form ventral structures, such as the ventral hole. However, the regenerated bone correctly re-patterns the ventral hole, implying that dorsal and ventral identities are conserved in the blastema during regeneration.[54]

Collectively our data demonstrate that at least one developmental limb patterning network is not re-used to regulate patterning during digit tip regeneration. However, En1 and Lmx1b only define the DV axis during limb development and there are two other axes (AP and PD) to consider. The digit tip bone is symmetrical in the AP axis, while there are morphological changes along the PD axis. Dermal fibroblasts, an important population in digit tip regeneration, retain positional information in the form of location-specific Hox expression, providing a Hox-dependent mechanism of positional memory.[66,67] Therefore, Hoxa13 and Hoxd13 are promising candidates that may direct morphogenesis in the PD and/or AP axes during digit tip regeneration as they do during limb development.[68-70] In contrast to loss of En1 or Lmx1b during development, which results in a quantifiable digit tip bone phenotype, loss of Hoxa13 or Hoxd13 during development does not result in a morphological change in the digit tip P3 bone but instead loss of certain digits,

loss of the P2 bone, and delayed development of digits overall.[69] However, Hoxd13 and Hoxa13 can also induce expression of osteogenic genes, such as Runx2, Bmp2, and Bmp7, coupling patterning and bone formation[24,71,72] and complicating interpretation of their role in regenerate patterning. By focusing on the DV axis in our study, we can distinguish between changes in bone regeneration and patterning, and between expression and function of developmental patterning genes during regeneration. Collectively, our data support the involvement of non-developmental mechanisms in patterning the mouse digit tip during regeneration. It is important to determine these patterning mechanisms because inducing regeneration in non-regenerative contexts, such as human limb regeneration, will require correct patterning of the regenerate.

Limitations of the study

We visualize and measure En1 or Lmx1b expression via mRNA, not protein. Technical limitations in the commercially available antibodies precluded protein analyses but, because mRNA and protein levels are not always perfectly correlated, these follow-up studies will be important as new reagents are developed.

We use limb development as a framework to study patterning during digit tip regeneration. We focus only on the DV axis and find that DV patterning in digit tip regeneration does not depend on the same factors as during limb development, En1 and Lmx1b. Our results show that there is a reproducible DV morphology in the regenerated digit tip, although we do not present data toward what controls it. Having overturned a widely accepted hypothesis of developmental patterning pathways being reused during regeneration, follow-up hypothesis-generating experiments to identify regeneration-specific patterning factors are necessary.

STAR★METHODS

RESOURCE AVAILABILITY

Lead contact—Further information and requests for resources and reagents should be directed to and will be fulfilled by the lead contact, Jessica Lehoczky (jlehoczky@bwh.harvard.edu) upon request.

Materials availability—This study did not generate new unique reagents.

Data and code availability

- All data reported in this paper will be shared by the lead contact upon request.
- This paper does not report original code.
- Any additional information required to reanalyze the data reported in this paper is available from the lead contact upon request.

EXPERIMENTAL MODEL AND SUBJECT DETAILS

Mice—Mouse (*Mus musculus*) husbandry and surgeries were done with the approval of the Brigham and Women's Hospital IACUC. e10.5 hindlimb, e12.5 brain, and fetal digit tips from male and female embryos were harvested from adult female pregnant CD1(ICR)

mice obtained from Charles River Laboratories (Cat #CRL:022). Neonatal digit tip tissue was obtained from CD1(ICR) 4- or 5-day old male and female mice. 6-week-old male and female FVB/NJ mice used for adult regenerating and unamputated digit tip tissue were obtained from The Jackson Laboratory (Cat #JAX:001800). To achieve En1 tissue specific knockout during development an En1 floxed allele[43] (Cat #JAX:007918) was used in combination with a K14-cre allele[44] to generate neonatal male and female mice for experimental cohorts (Cat #JAX:004782). En1 conditional knockout studies in adult 4 week old male and female mice used the same En1 floxed allele in combination with a K14-creERT2 allele[49] (courtesy of Dr. Pierre Chambon). To achieve Lmx1b mesenchymal specific knockout during development an Lmx1b floxed allele[45] (courtesy of Dr. Randy Johnson) was used in combination with a Prx1-cre allele[46] to generate neonatal male and female mice for experimental cohorts (Cat #JAX:005584). Lmx1b conditional knockout studies in adult 6 week old male and female mice used the same Lmx1b floxed allele in combination with an Msx1-creERT2 allele[51] (courtesy of Dr. Benoit Robert).

METHOD DETAILS

Mouse tamoxifen induction and digit tip amputation surgery—To induce recombination in 4-week-old En1-fl;K14-creERT2 and 6-week-old Lmx1b-fl;Msx1-creERT2 mice, tamoxifen (Sigma-Aldrich #T5648-1G) in corn oil was administered by oral gavage at 3 mg/40 g mouse body weight. Daily doses were administered on three consecutive days and digits were amputated the day after the last dose.

Neonatal digit amputations were performed for En1-flox;K14-cre and Lmx1b-flox;Prx1-cre experimental cohorts as previously described.[53,60] Postnatal day 3 pups were cryoanesthetized and hindlimb digits 2, 3, and 4 were amputated midway through the distal tip with micro-spring scissors. Pups were returned to the mother and digits regenerated until harvested as noted. Adult digit tip amputations were performed as previously reported.[27] FVB/NJ, En1-flox;K14-creERT2, or Lmx1b-flox;Msx1-creERT2 mice were anesthetized with 3–4% isoflurane and anesthesia was maintained at 2% isoflurane. Digits 2, 3, and 4 of the right and/or left hindlimb were visualized under a Leica S6E dissecting microscope and amputated distally. Mice were given buprenorphine at a dose of 0.05 mg/kg at time of surgery and again 8–12 h later, then monitored for 4 days.

Hybridization chain reaction RNA fluorescent *in situ* hybridization (HCR RNA-FISH)—Unamputated digit tissue from neonatal (PN4/5) CD1(ICR) mice was collected into ice cold 4% PFA for fixation overnight at 4C, washed with PBS, and then incubated in graded sucrose solutions from 5% to 30% over 3 days at 4C before embedding in OCT (Tissue-Tek). Unamputated embryonic (e10.5 or e12.5) and fetal (e16.5) limb bud or digit tissue was collected from timed pregnant CD1(ICR) females and treated as above with solution changes at 30 min instead of overnight. Adult unamputated or blastema stage digits from FVB/NJ, En1-flox;K14-creERT2, or Lmx1b-flox;Msx1-creERT2 mice were collected and treated in the same manner as neonatal digit tissue with the addition of a decalcifying step with Decalcifying Solution Lite (Sigma-Aldrich) at room temperature for 40 min before graded sucrose. All tissue was stored in OCT at −80C and then sectioned at 10 μm (fetal and neonatal) or 18 μm (adult) on a Leica CM3050S cryostat.

For HCR RNA-FISH, sections were prepared for probe hybridization as previously described[76] with the addition of Proteinase K (3ug/mL) for 10 min at room temperature. Probe hybridization and signal amplification followed the Molecular Instruments HCR v3.0 manufacturer's protocol for sections. Briefly, probes targeting mouse En1 (GenBank: NM_010133.2, full length cDNA or the floxed region of En1-flox), Lmx1b (GenBank: NM_010725.3), and Wnt7a (GenBank: NM_009527.4) were hybridized to tissue sections at 37C overnight. After probe washing, signal amplification hairpins were added to sections and amplified at room temperature overnight. After washing, the TrueVIEW autofluorescence quenching kit (Vector Laboratories) was used to quench endogenous fluorescence before sections were counterstained with DAPI at 1 ng/uL. To generate no probe control sections, sections were treated as above but no probe was added to the hybridization buffer. All *in situ* experiments were done minimally in duplicate on sections from different animals. Sections were imaged in 5–10μM z-stacks on a Zeiss LSM 880 confocal microscope at 20×, 40×, or 63×. Z-stack maximum projections were generated in ImageJ v.1.53c and brightness and contrast of pseudo colored magenta, green, and gray channels were adjusted independently in Adobe Photoshop v.23.4.1.

Skeletal staining and analysis—3wpa and control UA digits of Lmx1b-flox;Prx1-cre and En1-flox;K14-cre experimental cohorts were prepared with a standard alizarin red and alcian blue staining protocol as previously reported.[60,77] Briefly, digits were collected into 100% ethanol for dehydration, then incubated in staining solution (0.005% alizarin red, 0.015% alcian blue, 5% acetic acid, and 60% ethanol) at 37°C for 24 h. Digit tissue was cleared using a 2% potassium hydroxide at room temperature for 2 days, then taken through increasing concentrations of glycerol (25%, 50%, 75%, and 100%) and imaged on a Leica M165 FC stereo microscope with a Leica DFC7000 T camera attachment. Images were processed in ImageJ where length was manually measured in triplicate from the mid-proximal joint to the distal digit tip. Regenerated digit length was divided by the same animal's contralateral UA digit length to calculate percent regeneration.

Micro computed tomography (uCT) scanning and analysis—4wpa or UA digits from Lmx1b-flox;Msx1-creERT2 and En1-flox;K14-creERT2 experimental cohorts were collected and stored in 70% ethanol until scanning. A Scanco Medical uCT 35 system with an isotropic voxel size of 7μm was used to scan digits in 70% ethanol in a 7 mm diameter sample tube with an X-ray tube potential of 55 kVp, a 0.5 mm aluminum filter, an X-ray intensity of 0.145 mA, and an integration time of 600 ms per slice. Alizarin red stained 3wpa or UA developmental mutant digits from En1-flox;K14-cre mice were scanned in 25% glycerol with the same settings. Scans were then converted to DICOM image sets and imported into our image analysis software, which used the C programming language for low level functions and the IDL package (L3Harris Geospatial, Broomfield, CO) for the graphical user interface.[74,75] We first placed two seed points on the digit scans identifying the base and tip of the distal phalanx. This step was used both to identify the location of the distal phalanx on the scan and to determine a "bone axis", defined as the approximate direction of the digit. Next, we chose a grey scale threshold level optimized to isolate the distal phalanx from the other more proximal bones in the scan, and the total bone volume and length were calculated. The isolated digit tip bone was then rotated so that the bone

axis was aligned with one edge of the 3D image so we could view cross sections of the distal phalanx. Landmarks were then placed on the rotated 3D images, one marking the slice containing the most distal tip of the bone and the other at an indexed slice located at the most distal end of the ventral hole. Two landmarks were placed on the indexed slice to define the DV axis (Figure 6A, red points) from which two additional morphometric metrics were defined. A symmetry value was defined as the ratio of the areas above and below the midpoint axis, which was placed at 60% of the height of the digit at the index slice. This ratio was plotted for the length of the bone from the indexed slice to the end point (Figure 6). We also defined a measure of the height to width, referred to as an aspect ratio, which was calculated at fixed locations along the digit (Figure 5A). The previously defined DV axis at the index slice was used to measure the height of the bone at each slice, then a line perpendicular to the first line at 50% of the height was placed and the bone width measured. The aspect ratio was calculated as width divided by height. To fit segmented line (spline) models to V/D ratio values for each digit, we utilized the mcp package (v0.3.1) in R to infer two segments and one change point for each digit.[52] Ratio values for 0 to 75% of digit length were used as input to the model. We disregarded ratio values for the last 25% of the digit because morphology at the tip is variable, leading to ratio values of 0 or infinity for many digits.

Quantitative PCR (qPCR)—Digits 1 and 5 from experimental En1-flox;K14-creERT2 and Lmx1b-flox;Msx1-creERT2 animals were collected and stored at −20C until DNA extraction with the DNEasy Blood and Tissue kit (Qiagen) according to kit instructions. A standardized DNA concentration was used as input to qPCR reactions with primers that detect the En1 recombined allele (En1-fl;K14-creERT2 cohort) or the Lmx1b recombined allele (Lmx1b-fl;Msx1-creERT2 cohort). These primers span introns or intron-exon junctions and thus do not amplify En1 or Lmx1b mRNA. Primers for detecting recombination of the En1-floxed allele were 5’-GAGCTTGCGGAACCCTTAAT-3’ and 5’-GGTAGAGAAGAGGCGAGG-3′. Primers for detecting recombination of the Lmx1b-floxed allele were 5’-CAGCCCAATTCCGATCATATTCA-3’ and 5’-AAATACGGGGCTTTGGAACA-3′. SsoAdvanced Universal SYBR Green Supermix (Bio-Rad) was used to detect amplification of the target sequences on a QuantStudio 5 Real-Time PCR system (Applied Biosystems).

Quantitative reverse transcription PCR (RT-qPCR)—12dpa blastemas were microdissected from Lmx1b-fl;Msx1-creERT2 digit tips in PBS using super fine forceps as previously reported.[27] For each experimental group, two biological replicates of 12 blastemas from two to three mice were collected into RNA later (Thermo Fisher Scientific). RNA was then extracted using the RNeasy Plus Micro Kit (Qiagen) according to kit instructions and RNA concentrations were measured using a NanoDrop 1000 spectrophotometer (Thermo Fisher Scientific). A standardized amount of RNA from each sample was then used to generate cDNA using the SuperScript IV First-Strand Synthesis System (Thermo Fisher Scientific). Levels of Lmx1b cDNA were quantitatively measured using TaqMan Gene Expression Assay Mm01324882_g1 (Thermo Fisher Scientific) which spans the junction of exons 4 and 5, within the floxed portion of Lmx1b-fl[45] on a QuantStudio 5 Real-Time PCR system. Relative levels of expression were determined

using the ΔΔCT method using the Tbp TaqMan Gene Expression Assay Mm01277042_m1 (Thermo Fisher Scientific) as a housekeeping gene and the Lmx1b-fl/fl sample as the reference sample.

QUANTIFICATION AND STATISTICAL ANALYSIS

Quantification for each method is described in the corresponding STAR Methods section. Statistical analyses and plots were implemented in R (v4.1.2).[77] For all tests, p values < 0.05 were considered statistically significant. Significant p values are denoted as * if $p < 0.05$, ** if $p < 0.01$, and *** if $p < 0.001$.

For Figure 3, 15 En1-wt/wt;K14-cre, 8 En1-fl/fl;K14-cre, 15 Lmx1b-fl/wt;Prx1-cre and 6 Lmx1b-fl/fl;Prx1-cre digits were analyzed as noted in the figure. Data are represented using boxplots plotted in R (v4.1.2) using the ggplot2 package[78] where the center line corresponds to the median value, upper and lower edges of the box denote the 75th and 25th percentile values respectively, and the whiskers extend to the smallest and largest value within 1.5 times of the interquartile range. Individual points represent values for individual digits. A two-tailed t-test was used to determine statistical significance between groups.

For Figures 4, 5, 6, and S5, sample sizes for each group used in the length, volume, and spline analyses are as follows, where n refers to the number of individual digits in each group. UA: En1-fl/fl n = 48, En1-fl/fl;K14-creERT2 n = 24, En1-fl/fl;K14-creERT2+tam n = 28, En1-fl/fl + tam n = 12, Lmx1b-fl/fl n = 60, Lmx1b-fl/fl;Msx1-creERT2 n = 34, Lmx1b-fl/fl;Msx1-creERT2+tam n = 45. 4wpa: En1-fl/fl n = 48, En1-fl/fl;K14-creERT2 n = 22, En1-fl/fl;K14-creERT2+tam n = 27, En1-fl/fl + tam n = 11, Lmx1b-fl/fl n = 39, Lmx1b-fl/fl;Msx1-creERT2 n = 13, Lmx1b-fl/fl;Msx1-creERT2+tam n = 27. 6wpa: Lmx1b-fl/fl n = 23, Lmx1b-fl/fl;Msx1-creERT2 n = 23, Lmx1b-fl/fl;Msx1-creERT2+tam n = 14. For the circularity analysis, En1-fl/fl;K14-cre UA n = 10, En1-fl/fl;K14-cre 3wpa n = 7, UA En1-fl/fl n = 48, UA En1-fl/fl;K14-creERT2 n = 24, UA En1-fl/fl;K14-creERT2+tam n = 28, 4wpa En1-fl/fl n = 48, 4wpa En1-fl/fl;K14-creERT2 n = 22, 4wpa En1-fl/fl;K14-creERT2+tam n = 27. To test for statistically significant differences between groups for digit length, volume, and section circularity, significant two-way ANOVA tests were followed by a post-hoc Tukey HSD test with multi comparison correction. To test for statistically significant differences between groups for mean spline parameters, two-way MANOVA tests were followed with a two-way ANOVA and, if warranted, a Tukey HSD post-hoc test with multiple comparison correction. Adjusted p values are reported. Data are represented by boxplots as described above, except that individual dots represent outliers.

For Figure S4, qPCR data are represented by boxplots as described above with individual dots representing outliers. The number of individual digits in each group are as follows, as noted in the figure: En1-fl/fl = 2, En1-fl/fl +tamoxifen = 2, En1-fl/fl;K14-creERT2 = 11, En1-fl/fl;K14-creERT2+tamoxifen = 13, Lmx1b-fl/fl = 2, Lmx1b-fl/fl;Msx1-creERT2 = 13, Lmx1b-fl/fl;Msx1-creERT2+tamoxifen = 16. RT-qPCR data are presented as bar graphs of fold change, or $2^{-\Delta\Delta CT}$, with error bars representing the standard deviation of the two biological replicates. Statistical significance was determined by a one-way ANOVA test followed by a post hoc Tukey's T Test for pairwise comparisons as warranted. Adjusted p values are reported.

Supplementary Material

Refer to Web version on PubMed Central for supplementary material.

ACKNOWLEDGMENTS

We thank the NeuroTechnology Studio at Brigham and Women's Hospital for providing Zeiss LSM 880 confocal access and consultation on data acquisition. We also thank Dr. Anne Golding for Masson's trichrome histology. We are grateful to other members of the Lehoczky lab and Drs. Cliff Tabin, Marian Ros, and Kerby Oberg for helpful scientific discussions. This work was supported by the National Institutes of Health, Eunice Kennedy Shriver National Institute of Child Health and Human Development (R03HD093922 to J.A.L.), and funds from the Brigham and Women's Hospital Department of Orthopedic Surgery (J.A.L.).

REFERENCES

1. Johnson SL, and Weston JA (1995). Temperature-sensitive mutations that cause stage-specific defects in zebrafish fin regeneration. Genetics 141, 1583–1595. 10.1093/genetics/141.4.1583. [PubMed: 8601496]
2. Spallanzani L (1768). Prodromo di un' opera da imprimersi sopra le riproduzioni animali/(T. Becket and DeHondt). 10.5962/bhl.title.158642.
3. Illingworth CM (1974). Trapped fingers and amputated fingertips in children. J. Pediatr. Surg 9, 853–858. 10.1016/S0022-3468(74)80220-4. [PubMed: 4473530]
4. Zhao W, and Neufeld DA (1995). Bone regrowth in young mice stimulated by nail organ. J. Exp. Zool 271, 155–159. 10.1002/jez.1402710212. [PubMed: 7884389]
5. Borgens RB (1982). Mice regrow the tips of their foretoes. Science 217, 747–750. 10.1126/science.7100922. [PubMed: 7100922]
6. Carlson BM (1978). Types of morphogenetic phenomena in vertebrate regenerating systems. Am. Zool 18, 869–882. 10.1093/icb/18.4.869.
7. Hay ED, and Fischman DA (1961). Origin of the blastema in regenerating limbs of the newt Triturus viridescens. An autoradiographic study using tritiated thymidine to follow cell proliferation and migration. Dev. Biol 3, 26–59. [PubMed: 13712434]
8. Morgan TH (1901). Regeneration and liability to injury. Science 14, 235–248. 10.1126/science.14.346.235. [PubMed: 17806597]
9. Vieira WA, and McCusker CD (2019). Hierarchical pattern formation during amphibian limb regeneration. Biosystems 183, 103989–104041. 10.1016/j.biosystems.2019.103989. [PubMed: 31295535]
10. Flowers GP, and Crews CM (2020). Remembering where we are: positional information in salamander limb regeneration. Dev. Dynam 249, 465–482. 10.1002/dvdy.167.
11. Goss RJ (1969). Principles of Regeneration (Academic Press). 10.1016/c2013-0-12497-x.
12. Saunders JW (1948). The proximo-distal sequence of origin of the parts of the chick wing and the role of the ectoderm. J. Exp. Zool 108, 363–403. 10.1002/jez.1401080304. [PubMed: 18882505]
13. Summerbell D (1974). A quantitative analysis of the effect of excision of the AER from the chick limb-bud. J. Embryol. Exp. Morphol 32, 651–660. [PubMed: 4463222]
14. Lee J, Marrero L, Yu L, Dawson LA, Muneoka K, and Han M (2013). SDF-1α/CXCR4 signaling mediates digit tip regeneration promoted by BMP-2. Dev. Biol 382, 98–109. 10.1016/j.ydbio.2013.07.020. [PubMed: 23916851]
15. Storer MA, Mahmud N, Karamboulas K, Borrett MJ, Yuzwa SA, Gont A, Androschuk A, Sefton MV, Kaplan DR, and Miller FD (2020). Acquisition of a unique mesenchymal precursor-like blastema state underlies successful adult mammalian digit tip regeneration. Dev. Cell 52, 509–524.e9, e9. 10.1016/j.devcel.2019.12.004. [PubMed: 31902657]
16. Aztekin C, Hiscock TW, Gurdon J, Jullien J, Marioni J, and Simons BD (2021). Secreted inhibitors drive the loss of regeneration competence in Xenopus limbs. Development 148, dev199158. 10.1242/dev.199158. [PubMed: 34105722]

17. Boilly B, and Albert P (1990). In vitro control of blastema cell proliferation by extracts from epidermal cap and mesenchyme of regenerating limbs of axolotls. Roux's Arch. Dev. Biol 198, 443–447. 10.1007/BF00399054. [PubMed: 28305671]

18. Campbell LJ, and Crews CM (2008). Molecular and cellular basis of regeneration and tissue repair: wound epidermis formation and function in urodele amphibian limb regeneration. Cell. Mol. Life Sci 65, 73–79. 10.1007/s00018-007-7433-z. [PubMed: 18030417]

19. Ghosh S, Roy S, Séguin C, Bryant SV, and Gardiner DM (2008). Analysis of the expression and function of Wnt-5a and Wnt-5b in developing and regenerating axolotl (Ambystoma mexicanum) limbs. Dev. Growth Differ 50, 289–297. 10.1111/J.1440-169X.2008.01000.X. [PubMed: 18336582]

20. Satoh A, Graham GMC, Bryant SV, and Gardiner DM (2008). Neurotrophic regulation of epidermal dedifferentiation during wound healing and limb regeneration in the axolotl (Ambystoma mexicanum). Dev. Biol 319, 321–335. 10.1016/j.ydbio.2008.04.030. [PubMed: 18533144]

21. Endo T, Tamura K, and Ide H (2000). Analysis of gene expressions during Xenopus forelimb regeneration. Dev. Biol 220, 296–306. 10.1006/dbio.2000.9641. [PubMed: 10753517]

22. Roensch K, Tazaki A, Chara O, and Tanaka EM (2013). Progressive specification rather than intercalation of segments during limb regeneration. Science 342 (80), 1375–1379. 10.1126/science.1241796. [PubMed: 24337297]

23. Gardiner DM, Blumberg B, Komine Y, and Bryant SV (1995). Regulation of HoxA expression in developing and regenerating axolotl limbs. Development 121, 1731–1741. 10.1006/dbio.1998.8956. [PubMed: 7600989]

24. Takeo M, Chou WC, Sun Q, Lee W, Rabbani P, Loomis C, Taketo MM, and Ito M (2013). Wnt activation in nail epithelium couples nail growth to digit regeneration. Nature 499, 228–232, pii. 10.1038/nature12214nature12214. [PubMed: 23760480]

25. Gerber T, Murawala P, Knapp D, Masselink W, Schuez M, Hermann S, Gac-Santel M, Nowoshilow S, Kageyama J, Khattak S, et al. (2018). Single-cell analysis uncovers convergence of cell identities during axolotl limb regeneration. Science 362, eaaq0681. 10.1126/science.aaq0681. [PubMed: 30262634]

26. Qu F, Palte IC, Gontarz PM, Zhang B, and Guilak F (2020). Transcriptomic analysis of bone and fibrous tissue morphogenesis during digit tip regeneration in the adult mouse. Faseb. J 34, 9740–9754. 10.1096/fj.202000330R. [PubMed: 32506623]

27. Johnson GL, Masias EJ, and Lehoczky JA (2020). Cellular heterogeneity and lineage restriction during mouse digit tip regeneration at single-cell resolution. Dev. Cell 52, 525–540.e5. 10.1016/j.devcel.2020.01.026. [PubMed: 32097654]

28. Fernando WA, Leininger E, Simkin J, Li N, Malcom CA, Sathyamoorthi S, Han M, and Muneoka K (2011). Wound healing and blastema formation in regenerating digit tips of adult mice. Dev. Biol 350, 301–310. 10.1016/j.ydbio.2010.11.035. [PubMed: 21145316]

29. Marrero L, Simkin J, Sammarco M, and Muneoka K (2017). Fibroblast reticular cells engineer a blastema extracellular network during digit tip regeneration in mice. Regeneration 4, 69–84. 10.1002/reg2.75. [PubMed: 28616246]

30. Simkin J, Sammarco MC, Marrero L, Dawson LA, Yan M, Tucker C, Cammack A, and Muneoka K (2017). Macrophages are required to coordinate mouse digit tip regeneration. Development 144, 3907–3916. 10.1242/dev.150086. [PubMed: 28935712]

31. Cygan JA, Johnson RL, and McMahon AP (1997). Novel regulatory interactions revealed by studies of murine limb pattern in Wnt-7a and En-1 mutants. Development 124, 5021–5032. 10.1242/dev.124.24.5021. [PubMed: 9362463]

32. Loomis CA, Kimmel RA, Tong CX, Michaud J, and Joyner AL (1998). Analysis of the genetic pathway leading to formation of ectopic apical ectodermal ridges in mouse Engrailed-1 mutant limbs. Development 125, 1137–1148. [PubMed: 9463360]

33. Dreyer SD, Naruse T, Morello R, Zabel B, Winterpacht A, Johnson RL, Lee B, and Oberg KC (2004). Lmx1b expression during joint and tendon formation: localization and evaluation of potential downstream targets. Gene Expr. Patterns 4, 397–405. 10.1016/j.modgep.2004.01.006. [PubMed: 15183306]

34. Davis CA, Holmyard DP, Millen KJ, and Joyner AL (1991). Examining pattern formation in mouse, chicken and frog embryos with an Enspecific antiserum. Development 111, 287–298. 10.1242/dev.111.2.287. [PubMed: 1680044]
35. Lin MH, and Kopan R (2003). Long-range, nonautonomous effects of activated Notch1 on tissue homeostasis in the nail. Dev. Biol 263, 343–359. 10.1016/j.ydbio.2003.07.007. [PubMed: 14597207]
36. Kimura S, Schaumann BA, and Shiota K (2005). Ectopic dermal ridge configurations on the interdigital webbings of Hammertoe mutant mice (Hm): another possible role of programmed cell death in limb development. Birth Defects Res. A Clin. Mol. Teratol 73, 92–102. 10.1002/bdra.20108. [PubMed: 15678493]
37. Martin P (1990). Tissue patterning in the developing mouse limb. Int. J. Dev. Biol 34, 323–336. [PubMed: 1702679]
38. Choi HMT, Schwarzkopf M, Fornace ME, Acharya A, Artavanis G, Stegmaier J, Cunha A, and Pierce NA (2018).Third-generation *in situ* hybridization chain reaction: multiplexed, quantitative, sensitive, versatile, robust. Development 145, dev165753. 10.1242/dev.165753. [PubMed: 29945988]
39. Parr BA, Shea MJ, Vassileva G, and McMahon AP (1993). Mouse Wnt genes exhibit discrete domains of expression in the early embryonic CNS and limb buds. Development 119, 247–261. 10.1242/dev.119.1.247. [PubMed: 8275860]
40. Parr BA, and Mc Mahon AP (1995). Dorsalizing signal Wnt-7a required for normal polarity of D—V and A—P axes of mouse limb. Nature 374, 350–353. 10.1038/374350a0. [PubMed: 7885472]
41. Loomis CA, Harris E, Michaud J, Wurst W, Hanks M, and Joyner AL (1996). The mouse Engrailed-1 gene and ventral limb patterning. Nature 382, 360–363. 10.1038/382360a0. [PubMed: 8684466]
42. Chen H, and Johnson RL (2002). Interactions between dorsal-ventral patterning genes lmx1b, engrailed-1 and wnt-7a in the vertebrate limb. Int. J. Dev. Biol 46, 937–941. 10.1387/ijdb.12455631. [PubMed: 12455631]
43. Sgaier SK, Lao Z, Villanueva MP, Berenshteyn F, Stephen D, Turnbull RK, and Joyner AL (2007). Genetic subdivision of the tectum and cerebellum into functionally related regions based on differential sensitivity to engrailed proteins. Development 134, 2325–2335. 10.1242/dev.000620. [PubMed: 17537797]
44. Dassule HR, Lewis P, Bei M, Maas R, and McMahon AP (2000). Sonic hedgehog regulates growth and morphogenesis of the tooth. Development 127, 4775–4785. 10.1186/1471-2199-12-38. [PubMed: 11044393]
45. Zhao Z-Q, Scott M, Chiechio S, Wang J-S, Renner KJ, Gereau RW, Johnson RL, Deneris ES, and Chen Z-F (2006). Lmx1b is required for maintenance of central serotonergic neurons and mice lacking central serotonergic system exhibit normal locomotor activity. J. Neurosci 26, 12781–12788. 10.1523/JNEUROSCI.4143-06.2006. [PubMed: 17151281]
46. Logan M, Martin JF, Nagy A, Lobe C, Olson EN, and Tabin CJ (2002). Expression of Cre Recombinase in the developing mouse limb bud driven by a Prxl enhancer. Genesis 33, 77–80. 10.1002/gene.10092. [PubMed: 12112875]
47. Chen H, Lun Y, Ovchinnikov D, Kokubo H, Oberg KC, Pepicelli CV, Gan L, Lee B, and Johnson RL (1998). Limb and kidney defects in Lmx1b mutant mice suggest an involvement of LMX1B in human nail patella syndrome. Nat. Genet 19, 51–55. 10.1038/ng0598-51. [PubMed: 9590288]
48. Mohammad KS, Day FA, and Neufeld DA (1999). Bone growth is induced by nail transplantation in amputated proximal phalanges. Calcif. Tissue Int 65, 408–410. 10.1007/s002239900722. [PubMed: 10541769]
49. Li M, Indra AK, Warot X, Brocard J, Messaddeq N, Kato S, Metzger D, and Chambon P (2000). Skin abnormalities generated by temporally controlled RXRα mutations in mouse epidermis. Nature 407, 633–636. 10.1038/35036595. [PubMed: 11034212]
50. Dawson LA, Schanes PP, Kim P, Imholt FM, Qureshi O, Dolan CP, Yu L, Yan M, Zimmel KN, Falck AR, and Muneoka K (2018). Blastema formation and periosteal ossification in the regenerating adult mouse digit. Wound Repair Regen. 26, 263–273. 10.1111/wrr.12666. [PubMed: 30120800]

51. Lopes M, Goupille O, SaintCloment C, Lallemand Y, Cumano A, and Robert B (2011). Msx genes define a population of mural cell precursors required for head blood vessel maturation. Development 138, 3055–3066. 10.1242/dev.063214. [PubMed: 21693521]
52. Lindeløv JK (2020). mcp: an R package for regression with multiple change points. J. Stat. Software 10.31219/osf.io/fzqxv.
53. Lehoczky JA, Robert B, and Tabin CJ (2011). Mouse digit tip regeneration is mediated by fate-restricted progenitor cells. Proc. Natl. Acad. Sci. USA 108, 20609–20614. 10.1073/pnas.1118017108. [PubMed: 22143790]
54. Sammarco MC, Simkin J, Cammack AJ, Fassler D, Gossmann A, Marrero L, Lacey M, Van Meter K, and Muneoka K (2015). Hyperbaric oxygen promotes proximal bone regeneration and organized collagen composition during digit regeneration. PLoS One 10, 01401566–e140216. 10.1371/journal.pone.0140156.
55. Torok MA, Gardiner DM, Izpisúa-Belmonte JC, and Bryant SV (1999). Sonic Hedgehog (SHH) expression in developing and regenerating axolotl limbs. J. Exp. Zool 284, 197–206. 10.1002/(SICI)1097-010X(19990701)284:2<197::AID-JEZ9>3.0.CO;2-F. [PubMed: 10404648]
56. Han MJ, An JY, and Kim WS (2001). Expression patterns of Fgf-8 during development and limb regeneration of the axolotl. Dev. Dynam 220, 40–48. 10.1002/1097-0177(2000)9999:9999<::AID-DVDY1085>3.0.CO;2-8.
57. Rabinowitz JS, Robitaille AM, Wang Y, Ray CA, Thummel R, Gu H, Djukovic D, Raftery D, Berndt JD, and Moon RT (2017). Transcriptomic, proteomic, and metabolomic landscape of positional memory in the caudal fin of zebrafish. Proc. Natl. Acad. Sci. USA 114, E717–E726. 10.1073/pnas.1620755114. [PubMed: 28096348]
58. Shimokawa T, Yasutaka S, Kominami R, and Shinohara H (2013). Lmx-1b and Wnt-7a expression in axolotl limb during development and regeneration. Okajimas Folia Anat. Jpn 89, 119–124. 10.2535/ofaj.89.119. [PubMed: 23614984]
59. Takeo M, Hale CS, and Ito M (2016). Epithelium-derived wnt ligands are essential for maintenance of underlying digit bone. J. Invest. Dermatol 136, 1355–1363. 10.1016/j.jid.2016.03.018. [PubMed: 27021406]
60. Lehoczky JA, and Tabin CJ (2015). Lgr6 marks nail stem cells and is required for digit tip regeneration. Proc. Natl. Acad. Sci. USA 112, 13249–13254. 10.1073/pnas.1518874112. [PubMed: 26460010]
61. Lehoczky JA (2017). Are fingernails a key to unlocking the puzzle of mammalian limb regeneration? Exp. Dermatol 26, 478–482. 10.1111/exd.13246. [PubMed: 27761955]
62. Johnson GL, and Lehoczky JA (2022). Mammalian digit tip regeneration: moving from phenomenon to molecular mechanism. Cold Spring Harbor Perspect. Biol 14, a040857. 10.1101/cshper-spect.a040857.
63. Cesario JM, Landin Malt A, Chung JU, Khairallah MP, Dasgupta K, Asam K, Deacon LJ, Choi V, Almaidhan AA, Darwiche NA, et al. (2018). Anti-osteogenic function of a LIM-homeodomain transcription factor LMX1B is essential to early patterning of the calvaria. Dev. Biol 443, 103–116. 10.1016/j.ydbio.2018.05.022. [PubMed: 29852132]
64. Tang WJ, Watson CJ, Olmstead T, Allan CH, and Kwon RY (2022). Single-cell resolution of MET- and EMT-like programs in osteoblasts during zebrafish fin regeneration. iScience 25, 103784. 10.1016/j.isci.2022.103784. [PubMed: 35169687]
65. Haro E, Watson BA, Feenstra JM, Tegeler L, Pira CU, Mohan S, and Oberg KC (2017). Lmx1b-targeted cis-regulatory modules involved in limb dorsalization. Development 144, 2009–2020. 10.1242/dev.146332. [PubMed: 28455377]
66. Rinn JL, Bondre C, Gladstone HB, Brown PO, and Chang HY (2006). Anatomic demarcation by positional variation in fibroblast gene expression programs. PLoS Genet. 2, e119. 10.1371/journal.pgen.0020119. [PubMed: 16895450]
67. Rinn JL, Wang JK, Allen N, Brugmann SA, Mikels AJ, Liu H, Ridky TW, Stadler HS, Nusse R, Helms JA, and Chang HY (2008). A dermal HOX transcriptional program regulates site-specific epidermal fate. Genes Dev. 22, 303–307. 10.1101/gad.1610508. [PubMed: 18245445]

68. Dollé P, Dierich A, LeMeur M, Schimmang T, Schuhbaur B, Chambon P, and Duboule D (1993). Disruption of the Hoxd-13 gene induces localized heterochrony leading to mice with neotenic limbs. Cell 75, 431–441. 10.1016/0092-8674(93)90378-4. [PubMed: 8106170]
69. Fromental-Ramain C, Warot X, Messadecq N, LeMeur M, Dollé P, and Chambon P (1996). Hoxa-13 and Hoxd-13 play a crucial role in the patterning of the limb autopod. Development 122, 2997–3011. [PubMed: 8898214]
70. Kmita M, Tarchini B, Zàkàny J, Logan M, Tabin CJ, and Duboule D (2005). Early developmental arrest of mammalian limbs lacking HoxA/HoxD gene function. Nature 435, 1113–1116. 10.1038/nature03648. [PubMed: 15973411]
71. Yu L, Han M, Yan M, Lee E-C, Lee J, and Muneoka K (2010). BMP signaling induces digit regeneration in neonatal mice. Development 137, 551–559. 10.1242/dev.042424. [PubMed: 20110320]
72. Knosp WM, Scott V, Bächinger HP, and Stadler HS (2004). HOXA13 regulates the expression of bone morphogenetic proteins 2 and 7 to control distal limb morphogenesis. Development 131, 4581–4592. 10.1242/dev.01327. [PubMed: 15342482]
73. R Core Team (2018). R: A Language and Environment for Statistical Computing (Vienna, Austria: R Foundation for Statistical Computing). https://www.R-project.org/.
74. Duryea J, Magalnick M, Alli S, Yao L, Wilson M, and Goldbach-Mansky R (2008). Semiautomated three-dimensional segmentation software to quantify carpal bone volume changes on wrist CT scans for arthritis assessment. Med. Phys 35, 2321–2330. 10.1118/1.2900111. [PubMed: 18649465]
75. Charles JF, Sury M, Tsang K, Urso K, Henke K, Huang Y, Russell R, Duryea J, and Harris MP (2017). Utility of quantitative micro-computed tomographic analysis in zebrafish to define gene function during skeletogenesis. Bone 101, 162–171. 10.1016/j.bone.2017.05.001. [PubMed: 28476577]
76. Murtaugh LC, Chyung JH, and Lassar AB (1999). Sonic hedgehog promotes somitic chondrogenesis by altering the cellular response to BMP signaling. Genes Dev. 13, 225–237. 10.1101/gad.13.2.225. [PubMed: 9925646]
77. McLeod MJ (1980). Differential staining of cartilage and bone in whole mouse fetuses by alcian blue and alizarin red S. Teratology 22, 299–301. 10.1002/TERA.1420220306. [PubMed: 6165088]
78. Wickham H (2016). ggplot2: Elegant Graphics for Data Analysis (Springer International Publishing). 10.18637/jss.v035.b01.

Highlights

- En1 and Lmx1b are expressed in the regenerating digit tip, but without DV polarity
- Conditional deletion of En1 or Lmx1b modestly impairs bone regeneration
- Neither En1 nor Lmx1b are not required for DV patterning during digit tip regeneration
- DV limb patterning pathways are not re-used during digit regeneration

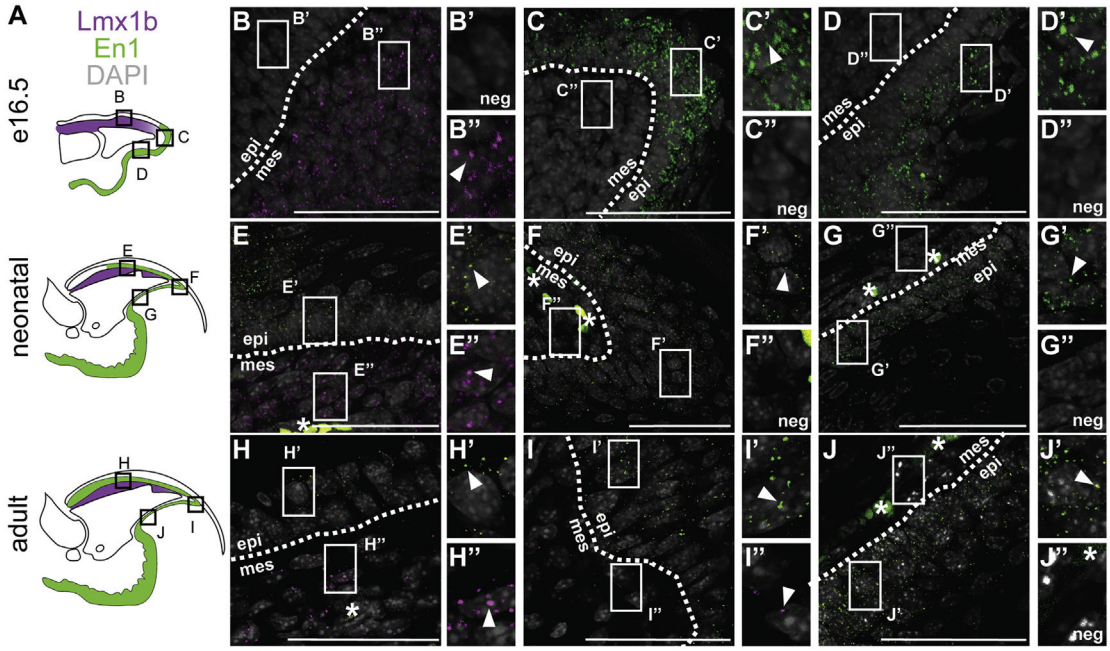

Figure 1. Expression of En1 and Lmx1b during digit tip development

(A) Schematics of mouse digit tip cross-sections at E16.5 (embryonic; top), PN4/5 (neonatal; middle), and 8 weeks old (adult; bottom), including En1 expression in green and Lmx1b expression in magenta. Lettered boxes correlate with position of *in situ* images on right.

(B–J) HCR RNA-FISH for En1 (green puncta) and Lmx1b (magenta puncta) in embryonic (B–D), neonatal (E–G), and adult (H–J) digit tip sections. DAPI is shown in grey. Arrowheads show examples of positive puncta; neg denotes no detected expression. Scale bars, 50 μm. Asterisks (*) denote blood vessel and red blood cell autofluorescence. Dashed lines show epithelial border. Epi, epithelium; mes, mesenchyme. Representative images from at least two biological replicates are shown. See also Figure S1.

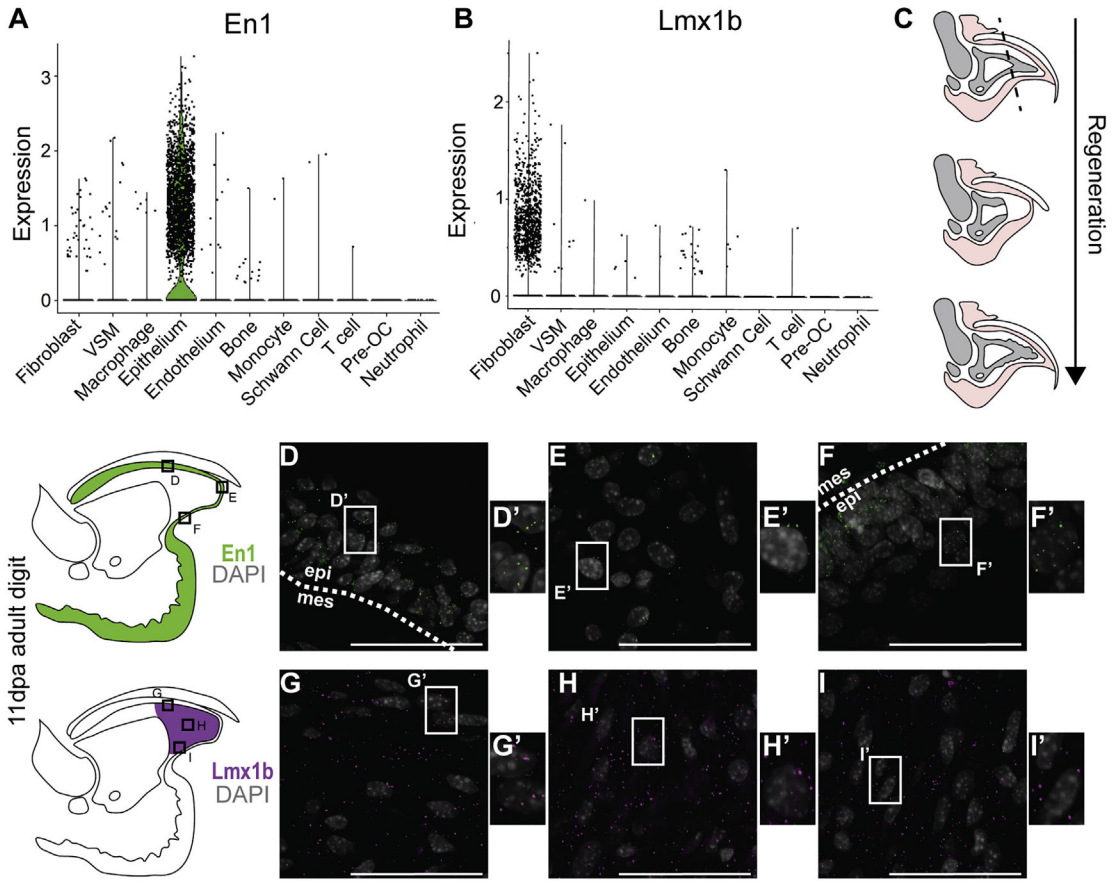

Figure 2. Expression of En1 and Lmx1b during digit tip regeneration

(A and B) Gene expression of En1 (A) and Lmx1b (B) in regenerating and unamputated digit tips shown by violin plot. Black dots represent individual cells.

(C) Schematic of mouse digit tip regeneration. Digits are amputated at the plane of the dashed line (top), resulting in blastema formation (middle) and regeneration of distal digit tip structures (bottom).

(D–I) HCR RNA-FISH for En1 (green puncta) (D–F) and Lmx1b (magenta puncta) (G–I) in 11 dpa regenerating digit tips. Schematics of mouse digit tip cross-sections at 11 dpa to the left include En1 expression in green and blastema-specific Lmx1b expression in magenta. Lettered boxes correlate with position of *in situ* images on right. DAPI is shown in grey. Scale bars, 50 μm. Dashed lines show epithelial border. Epi, epithelium; mes, mesenchyme. Representative images from at least two biological replicates are shown. See also Figures S2 and S3.

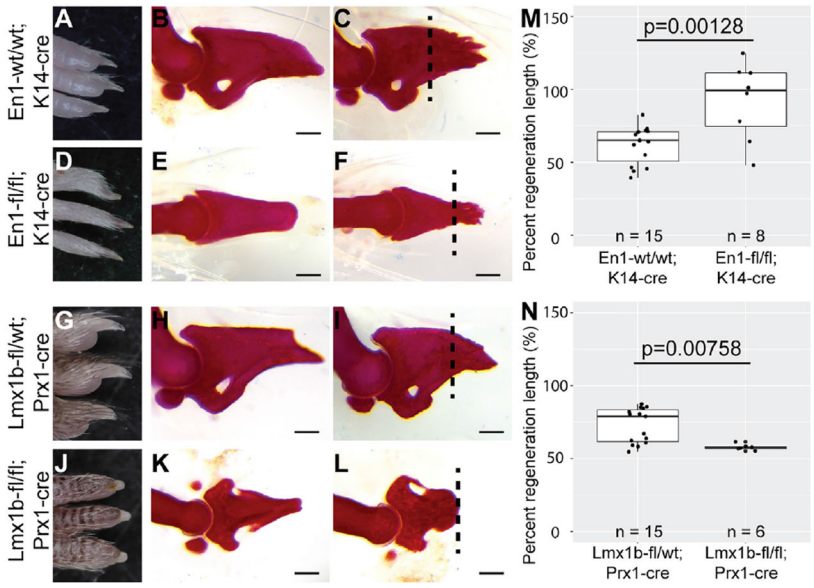

Figure 3. Developmental loss of En1 or Lmx1b perturbs digit tip regeneration

(A–C) Ventral view (A) of control En1-wt/wt;K14-cre digits and lateral view of alizarin red-stained unamputated (B) and 3 wpa (C) En1-wt/wt;K14-cre digit bones.

(D–F) Ventral view (D) of En1-fl/fl;K14-cre digits and lateral view of alizarin red-stained unamputated (E) and 3 wpa (F) En1-fl/fl;K14-cre digit bones.

(G–I) Dorsal view (G) of control Lmx1b-fl/wt;Prx1-cre digits and lateral view of alizarin red-stained unamputated (H) and 3 wpa (I) Lmx1b-fl/wt;Prx1-cre digit bones.

(J–L) Dorsal view (J) of Lmx1b-fl/fl;Prx1-cre digits and lateral view of alizarin red-stained unamputated (K) and 3 wpa (L) Lmx1b-fl/fl;Prx1-cre digit tip bones. Dashed lines denote amputation plane. Scale bars, 200 μm.

(M and N) Boxplot of digit tip bone percent regeneration length in En1-wt/wt;K14-cre or En1-fl/fl;K14-cre 3 wpa digits (M) or Lmx1b-fl/wt;Prx1-cre or Lmx1b-fl/fl;Prx1-cre 3 wpa digits (N). n = individual digits.

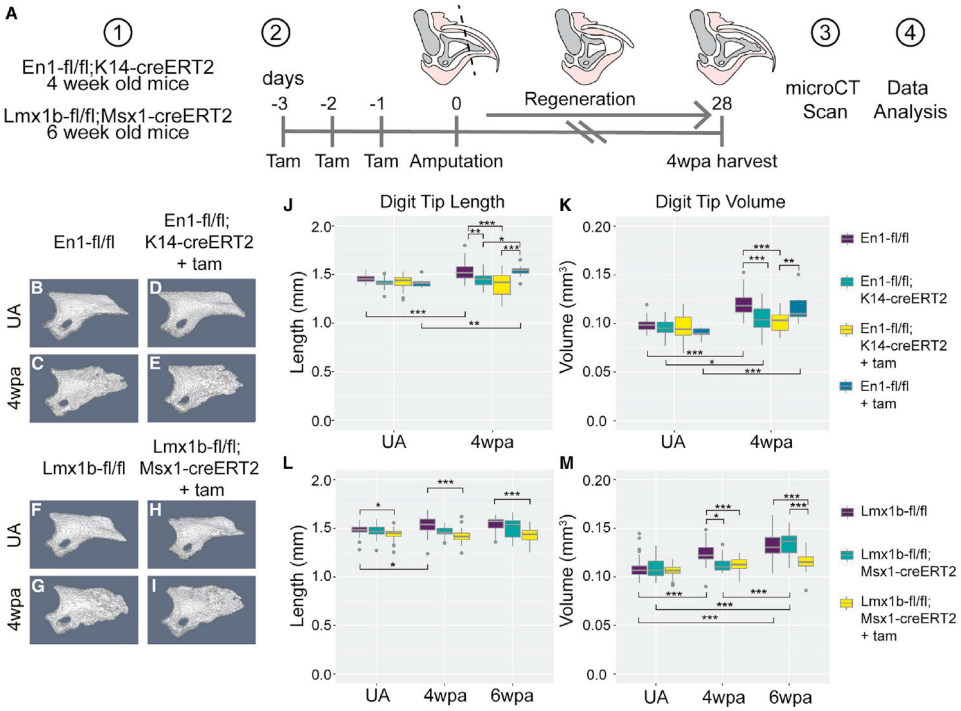

Figure 4. Conditional knockout of En1 and Lmx1b has a small effect on bone regeneration

(A) Schematic of the En1 and Lmx1b conditional knockout experiment.

(B–I) Representative 3D models of uCT scanned digits. (B and C) En1-fl/fl control UA (B) and 4 wpa (C) digits.

(D and E) En1-fl/fl;K14-creERT2 + tamoxifen UA (D) and 4 wpa (E) digits.

(F and G) Lmx1b-fl/fl control UA (F) and 4 wpa (G) digits.

(H and I) Lmx1b-fl/fl;Msx1-creERT2 + tamoxifen UA (H) and 4 wpa (I) digits.

(J–M) Boxplots showing quantification of digit length and volume for En1 control and +tamoxifen digits (J and K) and Lmx1b control and +tamoxifen digits (L and M). Number of individual digit tip bones in each group is noted in methods and Figure S5. *p < 0.05, **p < 0.01, ***p < 0.001. See also Figure S4.

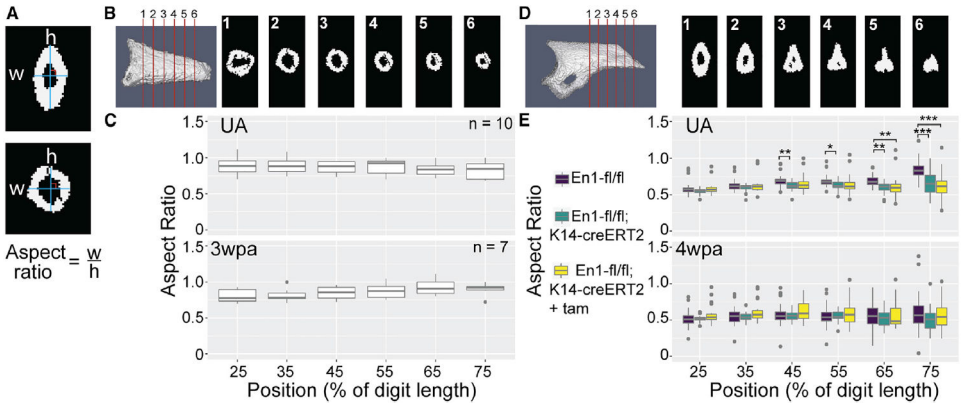

Figure 5. Loss of En1 during development, but not regeneration, increases circularity of the digit tip bone

(A) Example width and height measurements for slices shown in blue.

(B) Example 3D rendering of a neonatal En1-fl/fl;K14-cre digit. Numbered red lines indicate approximate position of correspondingly numbered slices through the digit bone.

(C) Boxplot of aspect ratio measurement for slices at 25%, 35%, 45%, 55%, 65%, and 75% of the length of the digit in unamputated (top) and 3 wpa (bottom) digits. n = individual digits.

(D) Example 3D rendering of an adult En1-fl/fl digit. Numbered red lines indicate approximate position of correspondingly numbered slices through the digit bone.

(E) Boxplot of aspect ratio measure for slices at 25%, 35%, 45%, 55%, 65%, and 75% of the length of the digit starting from the distal most part of the ventral hole in unamputated (top) and 4 wpa (bottom) digits. UA En1-fl/fl n = 48, UA En1-fl/fl;K14-creERT2 n = 24, UAEn1-fl/fl;K14-creERT2+tam n = 28. 4 wpa En1-fl/fl n = 48, 4 wpa En1-fl/fl;K14-creERT2 n = 22, 4 wpa En1-fl/fl;K14-creERT2+tam n = 27. n = individual digits. *$p < 0.05$, **$p < 0.01$, ***$p < 0.001$.

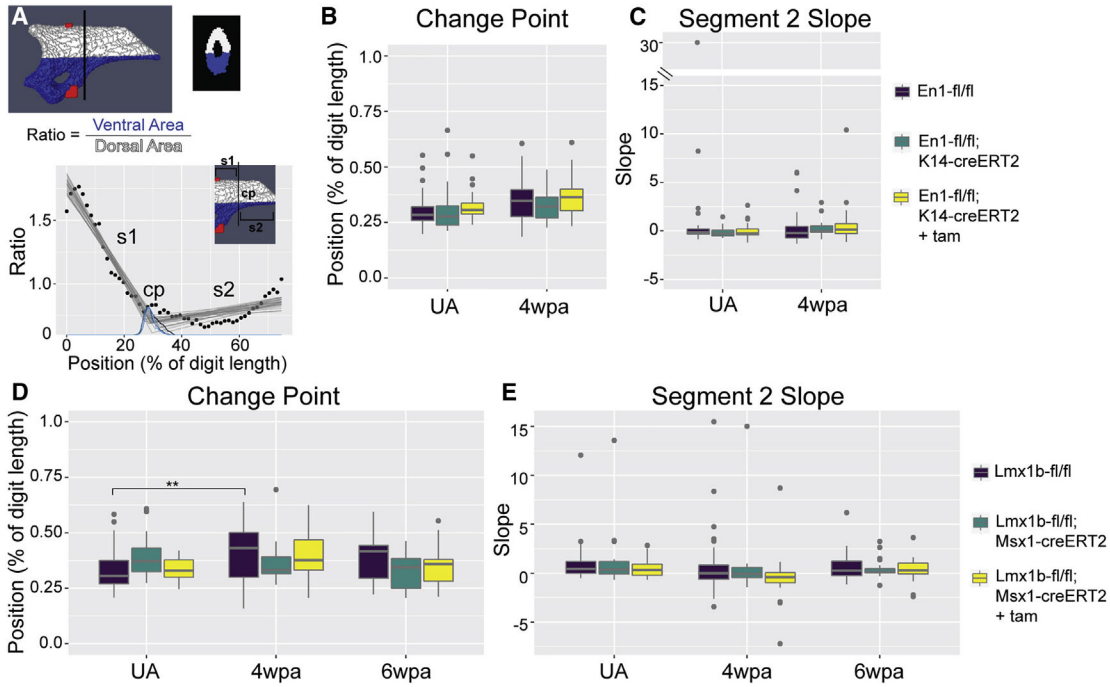

Figure 6. Conditional knockout of En1 or Lmx1b does not affect overall morphology of regenerated digit tip bones

(A) Schematic of data and analysis in (B–E). An unamputated digit is shown with dorsal area in white and ventral area in blue (top left), with a slice at the approximate position of the black line (top right). A ratio is computed by taking the ventral area divided by the dorsal area at many slices along the length of the digit. The plotted ratios (black points) are within the area shown by the inset, with the fitted model shown as gray lines. s1, first segment; cp, change point; s2, second segment.

(B and D) Boxplot showing mean change point predictions for each digit in the En1 (B) or Lmx1b (D) cohort.

(C and E) Boxplot showing mean slope predictions for the second segment for each digit in the En1 (C) or Lmx1b (E) cohort. Number of individual digit tip bones in each group is noted in STAR Methods and Figure S5. **p < 0.01.

KEY RESOURCES TABLE

REAGENT or RESOURCE	SOURCE	IDENTIFIER
Biological samples		
Embryos and neonatal and adult digit tips from CD1(ICR) mice, and adult digit tips from FVB/NJ mice	This paper	N/A
Neonatal digit tips from En1-flox;K14-cre and Lmx1b-flox;Prx1-cre mice. Strains described below.	This paper	N/A
Adult digit tips from En1-floxl;K14-creERT2 and Lmx1b-flox;Msx1-creERT2 mice. Strains described below.	This paper	N/A
Chemicals, peptides, and recombinant proteins		
Tamoxifen	Sigma-Aldrich	Cat# T5648-1G
Proteinase K	Sigma-Aldrich	Cat# 3115879001
Critical commercial assays		
Hybridization chain reaction v 3.0 probe hybridization buffer, probe wash buffer, and amplification buffer	Molecular Instruments	https://www.molecularinstruments.com/
HCR Probe Set: Mouse *En1* (Genbank: NM_010133.2) B4 hairpin compatible, 15 probe sets	Molecular Instruments	https://www.molecularinstruments.com/
HCR Probe Set: Mouse *Lmx1b* (Genbank: NM_010725.3) B1 hairpin compatible, 20 probe sets	Molecular Instruments	https://www.molecularinstruments.com/
HCR Probe Set: Mouse *Wnt7a* (Genbank: NM_009527.4) B2 hairpin compatible, 20 probe sets	Molecular Instruments	https://www.molecularinstruments.com/
HCR Probe Set: Mouse *En1* custom for a portion of exon 2. B5 hairpin compatible, 10 probe sets	Molecular Instruments	https://www.molecularinstruments.com/
HCR amplifier B2, Alexa Fluor 647 label	Molecular Instruments	https://www.molecularinstruments.com/
HCR amplifier B1, Alexa Fluor 647 label	Molecular Instruments	https://www.molecularinstruments.com/
HCR amplifier B4, Alexa Fluor 594 label	Molecular Instruments	https://www.molecularinstruments.com/
HCR amplifier B5, Alexa Fuor 647 label	Molecular Instruments	https://www.molecularinstruments.com/
TrueVIEW Autofluorescence Quenching Kit	Vector Laboratories	Cat# SP-8400
SsoAdvanced Universal SYBR Green Supermix	Bio-Rad	Cat# 1725271
SsoAdvanced Universal Probes Supermix	Bio-Rad	Cat# 1725281
Lmx1b TaqMan Gene Expression Assay (FAM), Mm01324882_g1	Thermo Fisher Scientific	Cat# 4351372
Tbp TaqMan Gene Expression Assay (VIC), Mm01277042_m1	Thermo Fisher Scientific	Cat# 4448485
DNEasy Blood and Tissue kit	Qiagen	Cat# 69504
RNeasy Plus Micro Kit	Qiagen	Cat# 74034
SuperScript IV First-Strand Synthesis System	Thermo Fisher Scientific	Cat# 18091050
Deposited data		
Raw scRNA-seq data for adult digit tip blastemas at 11dpa, 12dpa, 14dpa, or 17dpa and the unamputated digit tip	Johnson, Masias, and Lehoczky 2020[27]	GEO: GSE143888
Experimental models: Organisms/strains		
Mouse: CD1(ICR)	Charles River Laboratories	Cat# CRL:022
Mouse: FVB/NJ	The Jackson Laboratory	Cat# JAX:001800
Mouse: En1-flox	The Jackson Laboratory	Cat# JAX:007918

REAGENT or RESOURCE	SOURCE	IDENTIFIER
Mouse: Lmx1b-flox	Courtesy of Dr. Randy Johnson (PMID: 11044393); now available at The Jackson Laboratory	Cat#: JAX:031287
Mouse: K14-cre	The Jackson Laboratory	Cat#: JAX:004782
Mouse: Prx1-cre	The Jackson Laboratory	Cat#: JAX:005584
Mouse: K14-creERT2	Courtesy of Dr. Pierre Chambon (PMID: 11034212)	N/A
Mouse: Msx1-creERT2	Courtesy of Dr. Benoit Robert (PMID: 2163521)	N/A
Oligonucleotides		
Forward primer for qPCR detection of the recombined En1 fl allele: 5'-GAGCTTGCGGAACCCTTAAT-3'		
Reverse primer for qPCR detection of the recombined En1 fl allele: 5'-GGTAGAGAAGAGGCGAGG-3'		
Forward primer for qPCR detection of the recombined Lmx1b fl allele: 5'-CAGCCCAATTCCGATCATATTCA-3'		
Reverse primer for qPCR detection of the recombined Lmx1b fl allele: 5'-AAATACGGGGCTTTGGAACA-3'		
Software and algorithms		
R (version 4.1.2)	R Core Team, 2018[73]	https://www.r-project.org/; RRID:SCR_001905
Zen Image Acquisition and Processing software (Multiple versions)	Zeiss Microscope	https://www.zeiss.com/microscopy/int/products/microscope-software/zen.html; RRID:SCR_013672
Adobe Illustrator CC (version 26.3.1)	Adobe Systems	https://www.adobe.com/products/illustrator.html; RRID:SCR_010279
Adobe Photoshop CC (version 23.4.1)	Adobe Systems	https://www.adobe.com/products/photoshop.html; RRID:SCR_014199
ImageJ (Version 1.53c)	NIH	https://imagej.net/; RRID:SCR_003070
Custom uCT image analysis software	Duryea et al. 2008[74] Charles et al. 2017[75]	
Interactive Data Language	L3Harris Geospatial	https://www.l3harrisgeospatial.com/Software-Technology/IDL